

Effects of halogens on European air-quality

Journal:	<i>Faraday Discussions</i>
Manuscript ID	Draft
Article Type:	Paper
Date Submitted by the Author:	n/a
Complete List of Authors:	Sherwen, Tomás; University of York, Wolfson Atmospheric Chemistry Laboratories Evans, Mathew; University of York, Wolfson Atmospheric Chemistry Laboratories; University of York, National Centre for Atmospheric Science Sommariva, Roberto; University of Leicester Hollis, Lloyd; University of Leicester Ball, Stephen; University of Leicester Monks, Paul; University of Leicester, Department of Chemistry Reed, Christopher; Facility for Airborne Atmospheric Measurements Carpenter, Lucy; University of York, Lee, James; University of York, Chemistry Forster, Grant; University of East Anglia, School of Environmental Sciences; National Centre for Atmospheric Science (NCAS), University of East Anglia Bandy, Brian; National centre for atmospheric Science (NCAS), University of East Anglia; University of East Anglia Reeves, Claire; University of East Anglia, School of Environmental Sciences Bloss, William; University of Birmingham, School of Geography, Earth and Environmental Sciences

Supplement of

“Effects of halogens on European air-quality”

T. M. Sherwen et al.

This document contains two tables and five figures.

Table S11 - Scaling applied to VOC emissions used in simulation.

Species	Scaling
C₃H₈	2
Acetaldehyde	4
CH₂O	4
Acetone	1

Table footnote: The base emissions, prior to scaling, for C₃H₈ are assumed to be equivalent to C₂H₆ and acetaldehyde emissions are used to scale CH₂O and acetone emissions. A scaling of four is applied to acetaldehyde.

Table S12 - Definition of families.

Family	Definition
particulate matter less than 2.5 microns (PM_{2.5})	$1.51 * ([\text{NH}_4] + [\text{NIT}] + [\text{SO}_4]) + [\text{BCPI}] + [\text{BCPO}] +$ $1.2 * ((\text{OCPI} * 1.24) + \text{OCPO}) + [\text{DST1}] + 0.38 * [\text{DST2}] +$ $2.42 * [\text{SALA}]$

Table footnote: Definition of particulate matter less than 2.5 microns (PM_{2.5}) used here. Where “NIT”=nitrate aerosol, “BCPI”=Hydrophilic black carbon aerosol, “BCPO”=Hydrophobic black carbon aerosol, “OCPI”=Hydrophilic organic carbon aerosol, “OCPO”=Hydrophobic organic carbon aerosol, “DST1”=Dust aerosol (with R_{eff} = 0.7 microns), “DST2”=Dust aerosol, (R_{eff} = 1.4 microns), and “SALA”=Accumulation mode sea salt aerosol (R_{eff} = 0.1 – 2.5 microns). The scaling factors used assume an average RH of 50% for the domain.

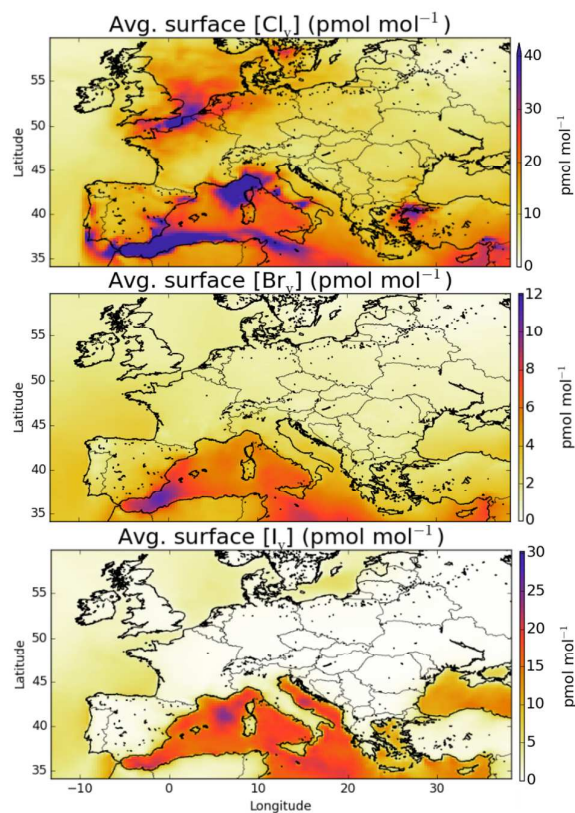


Figure S11 - Modelled surface mixing ratios/concentrations of X_y ($X=Cl, Br, I$) in “HAL” simulation for the summer observation period (2015/06/29-2015/08/01). Maximum values in figure are 27, 11 and 99 pmol mol^{-1} , for I_y , Br_y and Cl_y respectively. When X_y is the sum of inorganic halogens.

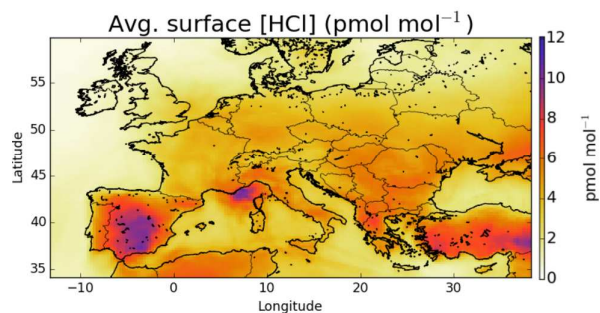


Figure S12 - Modelled surface mixing ratio of HCl in “HAL” simulation for the summer observation period (2015/06/29-2015/08/01) .

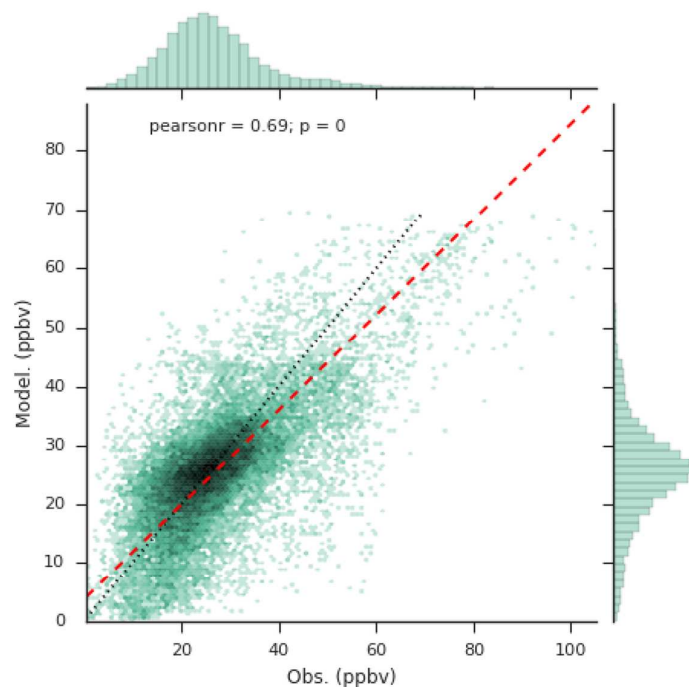


Fig. S13 Comparison of observed and modelled O_3 concentrations at UK AURN background sites ($N=63$) for the observation period (2015/06/29-2015/08/01). Red line shows orthogonal distance regression. Values are coloured in hexbins by log of number density, with probability distributions shown. Line of equality is shown in dashed black.

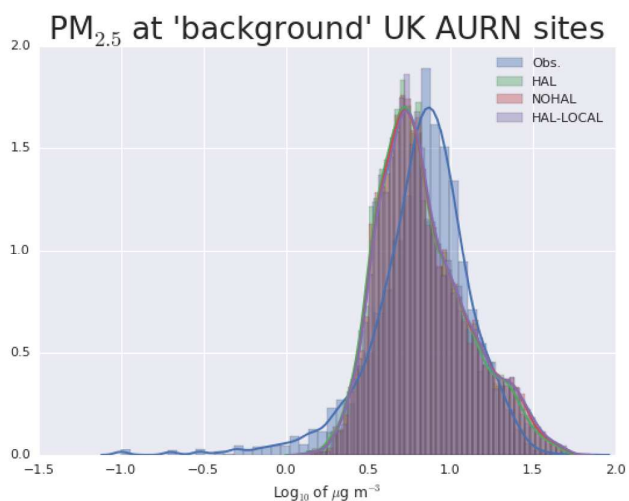


Fig. S14 Probability distribution function of the log of observed and modelled $PM_{2.5}$ concentrations at UK AURN background sites ($N=39$) for the observation period (29th June-1st August 2015). Values are shown for the simulation with halogens (“HAL”), without halogens (“NOHAL”), and with halogens only with the European domain (“LOCAL-HAL”).

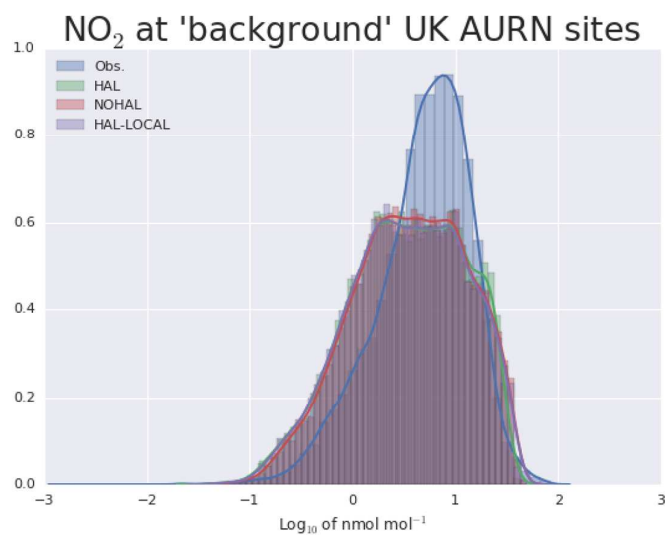


Fig. S15 Probability distribution function of the log of observed and modelled NO₂ concentrations at UK AURN background sites (N=62) for the observation period (29th June-1st August 2015). Values are shown for the simulation with halogens (“HAL”), without halogens (“NOHAL”), and with halogens only with the European domain (“LOCAL-HAL”).

T. Sherwen and M. Evans conceived and designed the model experiments, and wrote the paper. T. Sherwen performed the modelling experiments and analysed the model data.

R. Sommariva, L. D. J. Hollis, S. M. Ball, C. Reed, J. Lee, G. Forster, and B. Bandy collected and analysed the observational data. R. Sommariva, L. D. J. Hollis, S. M. Ball, P. S. Monks, C. E. Reed, L. J. Carpenter, J. D. Lee, G. Forster, B. Bandy, C. Reeves, and W. J. Bloss contributed materials/analysis tools and assisted in the writing of the paper.



Cite this: DOI: 10.1039/xxxxxxxxxx

Effects of halogens on European air-quality[†]

T. Sherwen,^{*a} M. J. Evans,^{a,b} R. Sommariva,^c L. D. J. Hollis,^c S. M. Ball,^c P. S. Monks,^c C. Reed,^{a‡} L. J. Carpenter,^a J. D. Lee,^{a,b} G. Forster,^{d,e} B. Bandy,^e C. E. Reeves,^e and W. J. Bloss^f

Received Date
Accepted Date

DOI: 10.1039/xxxxxxxxxx

www.rsc.org/journalname

Halogens (Cl, Br) have a profound influence on stratospheric ozone (O_3). They (Cl, Br and I) have recently also been shown to impact the troposphere, notably by reducing the mixing ratios of O_3 and OH. Their potential for impacting regional air-quality is less well understood. We explore the impact of halogens on regional pollutants (focussing on O_3) with the European grid of the GEOS-Chem model ($0.25^\circ \times 0.3125^\circ$). It has recently been updated to include a representation of halogen chemistry. We focus on the summer of 2015 during the ICOZA campaign at the Weybourne Atmospheric Observatory on the North Sea coast of the UK. Comparison between these observations together with those from the UK air-quality network show that the model has some skill in representing the mixing ratios/concentration of pollutants during this period. Although, the model has some success in simulating the Weybourne $ClNO_2$ observations, it significantly underestimates $ClNO_2$ observations reported at inland locations. It also underestimates mixing ratios of IO, OIO, I_2 and BrO , but this may reflect the coastal nature of these observations. Model simulations, with and without halogens, highlight the processes by which halogens can impact O_3 . Throughout the domain O_3 mixing ratios are reduced by halogens. In northern Europe this is due to a change in the background O_3 advected into the region, whereas in southern Europe this is due to local chemistry driven by Mediterranean emissions. The proportion of hourly O_3 above 50 nmol mol^{-1} in Europe is reduced from 46% to 18% by halogens. $ClNO_2$ from N_2O_5 uptake onto sea-salt, leads to increases in O_3 mixing ratio, but these are smaller than the decreases caused by the bromine and iodine. 12% of ethane and 16% of acetone within the boundary layer is oxidised by Cl. Aerosol response to halogens is complex with small ($\sim 10\%$) reductions in $PM_{2.5}$ in most locations. A lack of observational constraints, coupled to large uncertainties in emissions and chemical processing of halogens make these conclusions tentative at best. However, the results here point to the potential for halogen chemistry to influence air quality policy in Europe and other parts of the world.

^a Wolfson Atmospheric Chemistry Laboratory, University of York, York, UK.

^b National Centre for Atmospheric Science (NCAS), University of York, York, UK.

^c Department of Chemistry, University of Leicester, Leicester, UK

^d NCAS, School of Environmental Sciences, University of East Anglia, Norwich, UK

^e School of Environmental Sciences, University of East Anglia, Norwich, UK

^f School of Geography, Earth and Environmental Science, University of Birmingham, Birmingham, UK

[‡] now at Facility for Airborne Atmospheric Measurements (FAAM)

[†] Electronic Supplementary Information (ESI) available separately. See DOI: 10.1039/b000000x/

1 Introduction

Over the last decade, there has been increasing evidence, from both an observational and modelling perspective, that halogens (Cl, Br and I) play a role in determining the composition of the troposphere.¹ Different studies have emphasised either the regional impact of these species,^{2–5} or their global impact.^{6–13} They have also tended to focus on the chemistry of chlorine,^{3,14} iodine^{10,15} or bromine,^{6,8,11} with few studies investigating the coupled chemistry of all three.^{7,12}

The tropospheric chemistry of halogens is complex (see recent review by Simpson et al.¹ and references within) with significant uncertainties remaining, particularly in some aspects of the gas-phase chemistry of iodine and in the heterogeneous processing of all halogens. Interactions between the halogens and HO_x, NO_x, and volatile organic compounds (VOC) species leads to halogens having a pervasive influence throughout the tropospheric chemistry system.^{11,12} The chemistry of Br and I is thought to lead to reductions in O₃ and OH mixing ratios globally^{8,10–12} whereas the chemistry of Cl is thought to lead to both increases in O₃ due to more rapid oxidation of VOCs^{2,16} and decreases due to halogen nitrate hydrolysis reducing O₃ production (via decreasing NO_x).¹¹ However, the calculated magnitude of these impacts will be critically dependent on the emissions and chemistry of halogens used.

Both biogenic and anthropogenic sources of gas-phase halogen precursors exist, from a mix of oceanic, terrestrial, and anthropogenic sources.¹ The oceanic source of halocarbons can be spatially variable reflecting different ecosystems and driving processes. For example, areas of tidal sea-weed can have significant emissions of iodine precursor gases which vary with the tide state.^{17–23} For iodine, chemistry involving atmospheric ozone and ocean iodide within the surface micro-layer of the ocean leads to the emission of inorganic (HOI, I₂) species.^{24,25} Other sources of halogens into the troposphere can also occur such as direct emissions (e.g. HCl/Cl₂^{26,27}) or transport from the stratosphere.

The largest emission of bromine and chlorine into the atmosphere comes from sea-salt aerosol. However this aerosol phase chloride and bromide must be liberated by heterogeneous chemistry to become a gas-phase source. Different mechanisms allow for activation to the gas phase: acid displacement (e.g. HNO₃); uptake of N₂O₅ to sea-salt to liberate ClNO₂;²⁸ uptake of other halogen species (HOBr, HOI, BrNO₃, HOBr, etc) to liberate dihalogen species (ICl, IBr, Br₂, BrCl, Cl₂).^{1,29,30}

Measuring the concentration of reactive halogen species in the atmosphere is difficult due to their low mixing ratio and reactivity. Although there remains some debate, recent observations have demonstrated the pervasive existence of bromine and iodine species throughout the troposphere over oceanic regions by a range of techniques. Highest mixing ratios of these species have been found close to tidal sources^{17–23} but measurable mixing ra-

tios have been found in the remote ocean³¹ and in the upper troposphere.³²

Observations of reactive chlorine species are particularly sparse. However, a relatively large dataset of ClNO₂ observations have now been made^{28,33–38} which show a build up at night and then a rapid decrease (due to photolysis) at sunrise. The observations in polluted coastal regions are explicable through the uptake of N₂O₅ onto sea-salt.²⁸ However, high mixing ratios of ClNO₂ in continental regions have proved harder to explain due to the short lifetime of sea-salt in the atmosphere. Various explanations have been postulated ranging from non-oceanic sources of both natural and anthropogenic chlorine species,³⁵ to the movement of chlorine from sea-salt to fine mode sulfate aerosol via gas phase chemistry.²⁸

Previous model studies of Br and I chemistry have focussed predominantly on their global scale impacts.^{6,8,9,11,12} Whereas, studies of the impact of Cl have typically focussed on a smaller hemispheric or regional (air quality) scale.^{2–4} The combined impact of all halogens on the regional scale is less well explored. Here, we use a new version of the GEOS-Chem model, which includes a representation of halogen chemistry,¹² run in its regional grid configuration^{39–42} for Europe⁴³ to explore the roles that halogens may play in controlling European air quality with a focus on O₃. We focus on the summer of 2015 as this allows us access to an observational dataset made on the North Sea coast of the UK. We explore the model fidelity against this data and that offered from the UK air quality network. We explore the differing role of halogens in determining both O₃ concentrations through changes to regional scale chemistry and the hemisphere background. We then consider impacts of halogens on oxidation and contribution of atomic chlorine. The relative contribution of the halogen families on O₃ are then considered, and the impacts on aerosol concentrations. Finally we suggest future areas of research to allow better representation of the halogen chemistry of the atmosphere on a regional scale.

2 Experimental

2.1 Observations

The Integrated Chemistry of Ozone in the Atmosphere (ICOZA) campaign⁴⁴ at the Weybourne Atmospheric Observatory (52.95°N, 1.12°E,⁴⁵) was designed to examine the composition of the atmosphere and local chemical processes at a coastal site in the UK during the summer of 2015 (29th June–1st August). Weybourne is a World Meteorological Organisation (WMO) Global Atmospheric Watch (GAW) programme site. In addition to the standard observations (CO, and O₃), additional NO_x (NO, NO₂), total reactive nitrogen (NO_y), nitryl chloride (ClNO₂) and molecular chlorine (Cl₂) measurements were made during this period.

The NO, NO₂ and NO_y observations were made ~4 m above ground level. The NO and NO₂ measurements were made using

a dual channel Air Quality Design Inc. (Golden, Colorado, USA) chemiluminescent instrument equipped with a UV-LED photolytic NO_2 converter as described by Reed et al.^{44,46} NO_y was measured using a Thermo Environmental 42i TL NO_x analyser equipped with a molybdenum catalytic converter. A second high temperature (375°C) molybdenum converter was placed upstream directly at the gas inlet. Heated molybdenum catalysts have been shown to convert NO_y species such as PAN, HNO_3 and particulate nitrate into NO_2 .^{47–50} Limits of detection were $1.5 \text{ pmol mol}^{-1}$ and $1.9 \text{ pmol mol}^{-1}$ averaged over 1 minute for NO and NO_2 , and 50 pmol mol^{-1} averaged over 1 minute for NO_y .

Carbon monoxide (CO) observations are part of the National Centre for Atmospheric Sciences (NCAS) long-term measurement programme and O_3 observations are part of the Department for Environment, Food and Rural Affairs (DEFRA) Automatic Urban and Rural Network (AURN). It was measured by a Reduction Gas Analyser (RGA3, Trace Analytical, Inc., California, USA) to the WMO CO X2004 scale and O_3 was measured using UV absorption (TE49i, Thermo Fisher Scientific Inc.).

The observations of ClNO_2 and Cl_2 were made with the University of Leicester Chemical Ionization Mass Spectrometer (CIMS). The instrument, manufactured by THS Instruments (Georgia, USA), is based on the CIMS technique described by Slusher et al.,⁵¹ and is similar in configuration to the instrument used by Liao et al.⁵² The Leicester CIMS was calibrated for Cl_2 , using a certified standard by BOC ($5 \text{ } \mu\text{mol mol}^{-1}$ in nitrogen), and for ClNO_2 , using the methodology described by Thaler et al.⁵³ The detection limit was $8.5 \text{ pmol mol}^{-1}$ for Cl_2 and $5.1 \text{ pmol mol}^{-1}$ for ClNO_2 . The instrument and the measurements are discussed in more detail in Sommariva et al. (in prep.).

Wider UK air-quality observation data (O_3 , NO_2 , $\text{PM}_{2.5}$) from the DEFRA's AURN⁵⁴ was extracted for the period of observations using the OpenAir R package.⁵⁵

2.2 Modelling

We used the GEOS-Chem model (version 10, (<http://www.geos-chem.org>), which includes O_x , HO_x , NO_x , and VOC chemistry⁵⁶ and a mass based aerosol scheme.^{57,58} The model also has a representation of bromine and chlorine chemistry^{8,59}, which has updated further to include (Cl, Br, I) chemistry^{11,15} as described by Sherwen et al.¹² The chlorine scheme is described by Schmidt et al,¹¹ with additions described in Sherwen et al.¹⁵ including further reactions of chlorine and bromine with organics, ClNO_2 emission following N_2O_5 uptake on sea-salt,⁶⁰ and heterogenous iodine cycling to produce IX ($X=\text{Cl,Br}$).²⁹ The model is run without sea-salt de-bromination following Schmidt et al,¹¹ and does not contain acid displacement of chlorine or anthropogenic chloride sources. The halogen cross-sections and rates have been updated to latest NASA-JPL (15-10) recommendations.¹⁶

The model includes biogenic emissions (MEGAN⁶¹), biomass

burning (GFED⁶²), biofuel emissions,⁶³ and aerosols emissions (inc. dust,⁵⁷ sea-salt,⁵⁸, and Black and organic carbon⁶⁴) as well as NO_x from Lightning,⁶⁵ soils,⁶⁶ and aircraft.⁶⁷ For anthropogenic emissions, the model uses the Co-operative Programme for Monitoring and Evaluation of the Long-range Transmission of Air Pollutants in Europe (EMEP) emissions (<http://www.emep.int>) for NO_x ,⁶⁸ SO_x ,⁶⁹ CO , and NH_3 for the latest available year (2013). EMEP anthropogenic VOC emissions are also used here, but for 2012. Emissions for formaldehyde and acetone were scaled from the EMEP acetaldehyde emissions, ethane emissions were scaled from the EMEP propane emission, and a scaling factor was applied to the acetaldehyde emission following the approach taken previously in Dunmore et al.⁷⁰ and described in table S11 in the supplementary information.

The halogen emissions used are as described in Sherwen et al.¹² Emissions of organic iodine species are taken from the monthly values of Ordonez et al⁷¹ at $1 \times 1^\circ$. Emissions of inorganic iodine (I_2 , HOI) use the parameterisation of Carpenter et al.,²⁴ which describes a dependency on model parameters of surface O_3 mixing ratio, wind speed, and ocean surface iodide concentration. Ocean surface iodide concentrations are parameterised based on sea-surface temperatures following MacDonald et al.²⁵ Coastal and tidal processes are not considered here, and the $1 \times 1^\circ$ resolution of the organic emissions cannot be expected to capture very localised halogen sources.

The GEOS-Chem model is run at two resolutions. A global simulation ($4 \times 5^\circ$) generates boundary conditions to allow “nesting” of a domain at a $\sim 25 \text{ km}$ ($0.25 \times 0.3125^\circ$) resolution covering a domain ($32.75\text{--}61.25^\circ\text{N}$, $-15\text{--}40^\circ\text{E}$) over Europe. The global model is run for two years (1^{st} January 2004– 1^{st} January 2006) with the first year discarded as “spin up”. Using the March 1st 2005 concentrations fields for March 1st 2015, the global model is run for three further months of “spin up” and to cover the observational period in order to generate boundary conditions. The regional model is then run from two weeks prior to the observational period (as “spin up”), before running for the campaign period (29^{th} June– 1^{st} August 2015) using the boundary conditions generated by the global model.

$\text{PM}_{2.5}$ is calculated from the model based on the mass of sulfate, nitrate, ammonia, hydrophilic and hydrophobic carbon, seasalt and dust, assuming relative humidity of 50 %. The coarse mode sea-salt and the two largest dust size bins are ignored for the calculation. We have not used the model's secondary organic aerosol scheme in these model simulations. A full description of the $\text{PM}_{2.5}$ calculation is given in supplementary information table S12.

Model runs performed are described in Table 1. Simulations were performed with halogen chemistry switched on (“HAL”) and off (“NOHAL”) in both the global (to generate the boundary conditions) and regional model. A simulation was also performed using the boundary conditions calculated with the halo-

gens switched off but with the halogen chemistry in the European domain switched on (“HAL-LOCAL”). A final simulation (“NOCINO₂”) was performed with halogen chemistry in both the regional and local version of the model but with the uptake of N₂O₅ uptake on sea-salt aerosol leading to the production of 2HNO₃ rather than HNO₃ + ClNO₂.

Table 1 Model runs

Abbreviation	Regional model chemistry	Boundary condition
HAL	Halogens on.	Halogens on.
NOHAL	Halogens off.	Halogens off.
HAL-LOCAL	Halogens on.	Halogens off.
NOCINO ₂	Halogens on. No ClNO ₂ production	Halogens on.

3 Model performance

Figure 1 shows the averaged modelled (“HAL”) surface distribution of O₃, NO₂, CO and PM_{2.5} for the period from 29th July to 1st August 2015. Highest O₃ mixing ratios are evident in southern Europe and over the Mediterranean, with evidence for a reduction in O₃ mixing ratios over the northern cities compared to the rural values due to reaction of O₃ with NO. NO₂ mixing ratios are spatially variable reflecting its short lifetime, with cities and ship tracks evident. CO mixing ratios are similar to those from NO₂ but are more diffusive and don’t show the ship tracks. The distribution of PM_{2.5} shows similarities to the CO and NO₂ reflecting common sources.

There are fewer studies assessing the performance of the European grid version of the GEOS-Chem model against observations⁴³ than for the model’s other regional variants (e.g. North American,^{41,42} China^{39,40}). Future studies are required to evaluate the model against observations more comprehensively. The AirBase dataset⁷² is well suited for this task but this data is not currently available for 2015. Instead here we make some provisional assessment of the model against two observations datasets of standard air quality pollutants. First, against a sub-set of observations made at Weybourne as part of the Integrated Chemistry of Ozone in the Atmosphere (ICOZA) campaign and secondly against the observations made as part of the UK AURN network. Once we have evaluated the model against these compounds we turn our attention to its simulation of halogen compounds

3.1 General model performance

A comparison between a sub-set of the observations (O₃, CO, NO_x and NO_y) made as part of the ICOZA campaign and the model (“HAL”) are shown as a time-series in Figure 2 and as an average diel cycle in Figure 3. The model captures much of the observed synoptic timescale variability in these species. Notable exception include the failure to simulate the very high O₃ mixing ratios occurring at the start of the campaign and the high CO mixing ratios in the middle of the campaign. The diel average shows

a reasonable ability to reproduce the daily signal in these compounds other than for CO where the model shows a significantly larger cycle than is observed. The model has an average low bias (“HAL”-Obs.)/Obs.) of 9.2, 0.7, 2.5, and 11 %, for O₃, NO_x, NO_y and CO respectively.

To give a wider geographical comparison, the model (“HAL”) was compared against hourly O₃, PM_{2.5}, and NO₂ observations from the UK AURN air quality network.⁵⁴ Sites reporting data and classed as “rural”, “rural background” or “urban background” by DEFRA are used for the comparison. Sites influenced by localised emissions (e.g. roadside sites) are excluded as they are unlikely to provide an appropriate comparison for a model run at 0.25° resolution. A point-by-point comparison between the hourly measured and the spatially and temporally equivalent model values for O₃ is given in the supplementary figure SI3. The model fails to capture peak O₃ mixing ratios, which could be expected considering the limited reactive organics present in the model and could also contribute towards the slight underestimate in average O₃ mixing ratios between observation and the “HAL” simulation shown in Figure 3.

The probability distribution of the O₃ observations, and the model simulation for the AURN sites for the “HAL”, “NOHAL”, “HAL-LOCAL” simulations are shown in Figure 4 (with equivalent log plots shown for PM_{2.5} and NO₂ in the supplementary figures SI4 and SI5). The model without halogen chemistry in either the boundary conditions or in the region (“NOHAL”) shows substantially higher mixing ratios of O₃ (mean of 34.5 nmol mol⁻¹, 25th percentile=28.5 nmol mol⁻¹ and 75th percentile=41.1 nmol mol⁻¹) than observed (mean=27.0 nmol mol⁻¹, 25th percentile=19.0 nmol mol⁻¹ and 75th percentile=32.8 nmol mol⁻¹). The model without the halogen chemistry in the boundary conditions (“HAL-LOCAL”) calculates similarly higher O₃ mixing ratios. However, including halogen chemistry in both the boundary conditions and in the domain leads to a substantial decrease in the modelled O₃ mixing ratios (mean reduction of 26.1 %) improving the simulation (mean=25.5 nmol mol⁻¹, 25th percentile=19.5 nmol mol⁻¹ and 75th percentile=31.1 nmol mol⁻¹).

Unlike for O₃, where large changes are seen on inclusion of halogens, modest changes are seen for NO₂ and PM_{2.5} (Supplementary plots SI7 and SI8). For NO₂ the mean hourly modelled mixing ratio for the “HAL” simulation is 6.7 (25th percentile=1.4 and 75th percentile=9.5) nmol mol⁻¹ whereas the mean in the “NOHAL” simulation is 7.1 nmol mol⁻¹. Both can be compared to the observational mean of 7.7 (25th percentile=2.6 and 75th percentile=10.4) nmol mol⁻¹. For the PM_{2.5} the modelled “HAL” mixing ratio was 8.2 (25th percentile=4.2 and 75th percentile=9.7) μg m⁻³ with a “NOHAL” mean of 8.6 (25th percentile=4.3 and 75th percentile=10.0) and an observed concentration of was 8.0 (25th percentile=4.6 and 75th percentile=10.0)

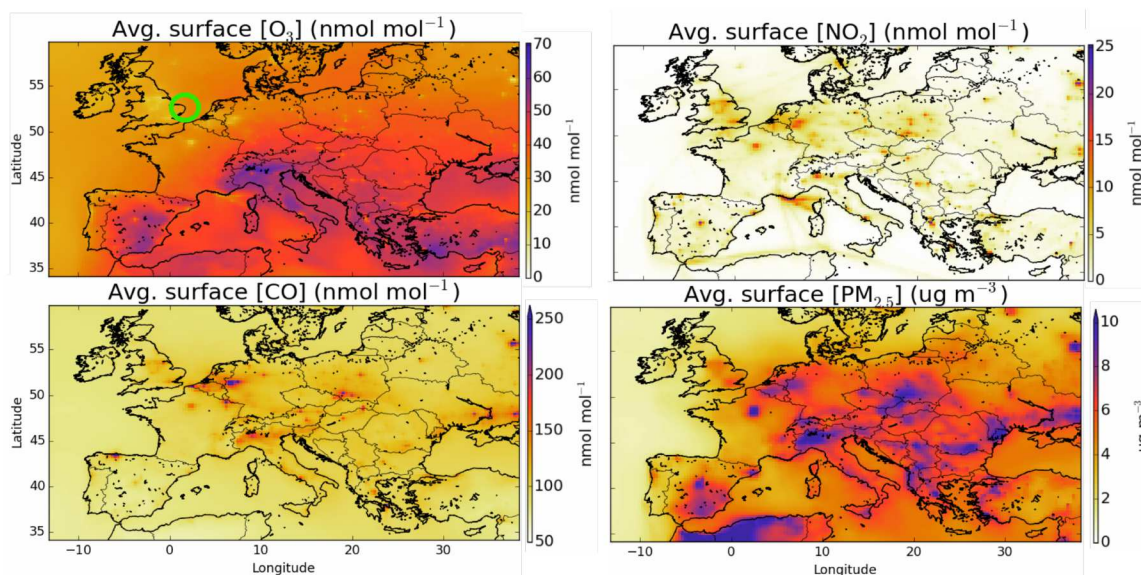


Fig. 1 Mean modelled surface O_3 , NO_2 , CO , and $\text{PM}_{2.5}$ mixing ratios / concentrations for the observational period (29th June-1st August 2015). The green circle on the first plot gives the location of the Weybourne Atmospheric Observatory. Maximum values in plots of CO and $\text{PM}_{2.5}$ are $431 \text{ pmol mol}^{-1}$ and $35 \mu\text{g m}^{-3}$, respectively.

$\mu\text{g m}^{-3}$.

We now turn our attention from the model's ability to simulate inorganic halogen compounds over Europe.

3.2 Model simulations of reactive halogens in Europe

The simulation of halogens in the global version of GEOS-Chem and its comparison with observations is discussed previously.^{11,12} This provided a first broad-brush assessment of the mixing ratio of halogens (mainly IO and BrO). It concluded that the model appears to have some skill in simulating IO and BrO mixing ratios but appears to underestimate Cl species.

Mean surface mixing ratios of key reactive halogens (BrO, IO and Cl) over Europe are shown in Figure 5 with mixing ratios of total inorganic halogens (X_y , $X=\text{Cl, Br, I}$) given in the supplementary information (SI1). We model the highest halogen mixing ratios over the Mediterranean where emissions are greatest. These emissions are notably high for iodine species where the elevated O_3 together with high sea-surface temperature (which determines the ocean iodide mixing ratio in our simulations^{24,25}) leads to a large inorganic iodine flux. A notable difference exists for Cl_y (Figure SI1) where a peak can be also be seen in the North Sea/English channel where high mixing ratios of sea-salt and NO_x leads to high ClNO_2 production.

Observations of bromine and iodine inorganic species have previously been reported for a few boundary layer locations in Europe, for example Ireland,^{17,18} France,^{19–22,73} and Spain.²³ We now compare values reported in the literature to the values calculated in our model for the period of the simulation (for 29th

June-1st August 2015). There are undoubtedly, large seasonal and inter-annual variability in these observations, but this comparison allows a rough assessment of the order of magnitude performance of the model.

A number of field campaigns have occurred over or near tidal coastal zones. IO has been observed at coastal Ireland (Mace Head, 53.3°N , -9.9°E) with peak mixing ratios of between 4 and 50 pmol mol^{-1} .^{74,75} The model predicts a maximum mixing ratio of $0.6 \text{ pmol mol}^{-1}$ here, substantially lower than the observations. IO has also been reported for Brittany (France, 48.7°N , -4.0°E) of between $7.7(\pm 0.5)$ ⁷⁶ and $30(\pm 7)$ ⁷³ pmol mol^{-1} and we again calculate lower values with a maximum of $0.07 \text{ pmol mol}^{-1}$. Observations 3.5km inland in Greece (Heraklion, 35.3°N , 25.1°E) report values less than $1.9(\pm 0.8) \text{ pmol mol}^{-1}$.⁷⁷ The model predicts a maximum mixing ratio of $1.8 \text{ pmol mol}^{-1}$ with an average below the stated limit of detection of the observations ($1.3 \text{ pmol mol}^{-1}$). Peters et al¹⁸ report peak IO observations in Germany (Dagebüll, 54.7°N , 8.7°E) of $2.0 (\pm 0.7) \text{ pmol mol}^{-1}$ and Oetjen⁷⁷ for nearby Sylt report a maximum of $1.4 \text{ pmol mol}^{-1}$. For Sylt and Dagebüll we peak mixing ratios of 1.8 and $0.7 \text{ pmol mol}^{-1}$, respectively.

Mixing ratios of IO have been measured by a ship cruise in the marine boundary layer of between 0.4 and 1 pmol mol^{-1} (30 % uncertainty).³¹ This cruise did not extend into the Mediterranean region (where we predict highest IO mixing ratios see Fig. 5), but it did finish in the Mediterranean at Cartagena (Spain) in July 2011 with the last daytime average value reported of $\sim 0.5 \text{ pmol mol}^{-1}$ (35°N , -8.4°E). For the same location we calculate

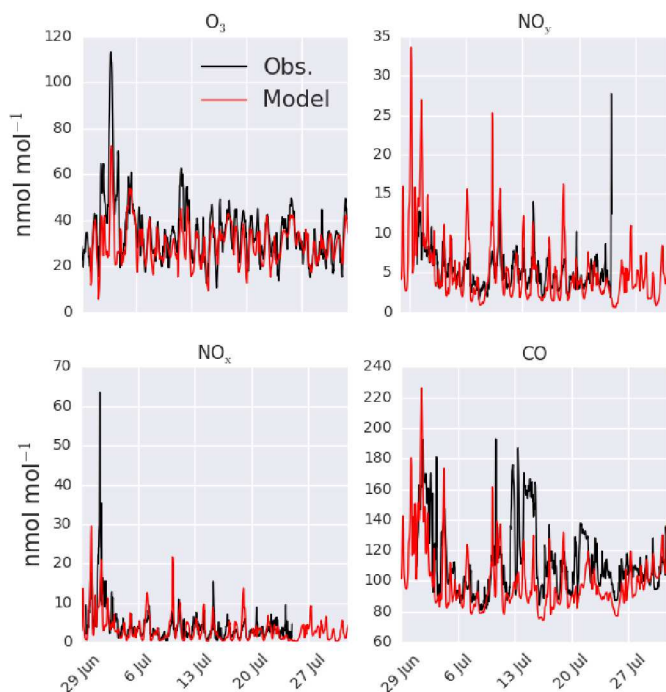


Fig. 2 Modelled (“HAL”) and observed mixing ratio at Weybourne of O_3 , NO_y , NO_x and CO during the observational period.

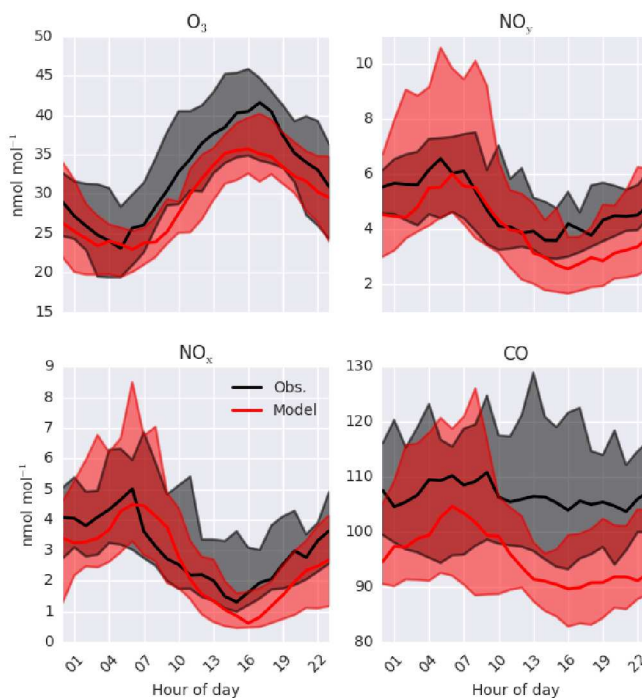


Fig. 3 Modelled (“HAL”) and observed median diel mixing ratio at Weybourne of O_3 , NO_y , NO_x and CO during the observational period. Shaded regions give 25th and 75th percentiles.

an average daytime mixing ratio of $0.7 \text{ pmol mol}^{-1}$.

Observations of iodine dioxide (OIO) have also been reported. At Mace Head, peak OIO mixing ratios have been reported (at night) of between $3.0 (\pm 0.4)^{78}$ and $13 (\pm 4) \text{ pmol mol}^{-1,76}$. The model predicts substantially lower peak values, of $0.09 \text{ pmol mol}^{-1}$. OIO mixing ratios have also been reported in Coastal France (Brittany, 48.7°N , -4.0°E) of around $9 \text{ pmol mol}^{-1,19}$ and with the model calculating significantly lower mixing ratios, peaking at $\text{peak}=0.007 \text{ pmol mol}^{-1}$.

Molecular I_2 has also been observed in Europe in coastal locations including Ireland, Spain and France. In Spain, (42.5°N , -8.9°E) mixing ratio were reported of $300 (\pm 100) \text{ pmol mol}^{-1}$. At Mace Head, peak nighttime mixing ratio of between $61 (\pm 20)^{18}$ to $94 (\pm 20)^{76} \text{ pmol mol}^{-1}$ have been reported and even higher values at nearby Mweenish Bay (53.3°N , -9.8°E)⁷⁹ have been found. In France (18.7°N , -8.87°E) mixing ratios of around 50 pmol mol^{-1} were observed.^{19,21} For these locations we calculate far lower maximum mixing ratios of 0.06, 0.04, 0.06, and 0.07 pmol mol^{-1} , respectively.

In summary, the model significantly under-predicts reported reactive iodine mixing ratios (IO, OIO, I_2) at coastal regions. The most active chemistry in the model occurs in the non-coastal Mediterranean (Fig. 5), a region where we are unaware of pub-

lished inorganic iodine observations.

Similarly to iodine, only a few bromine observations have been reported for Europe. At Mace Head and Brittany maximum mixing ratios were reported of 6.5^{80} and $7.5^{20} \text{ pmol mol}^{-1}$. For these locations we predict maximum mixing ratios of 0.8 and 0.5 pmol mol^{-1} , respectively. Lesser et al.⁸¹ reported measurements for a ship cruise from Germany to Capetown in October 2000, which included passing through the English Channel and to the west of Spain. Maximum values were reported of $2.4 \text{ pmol mol}^{-1}$ north of the Canary Islands and a similar value where the English Channel meets the Bay of Biscay. However the rest of the campaign did not report values above the detection limit. For the period the model was run, we predict average daytime mixing ratio below $\sim 0.3 \text{ pmol mol}^{-1}$ in regions of this campaign and even lower mixing ratios in areas with shipping emissions.

Figure 6 shows the observed and modelled time-series and median diel cycle of $ClNO_2$ mixing ratios at the Weybourne in Summer 2015. The observations show a large variability throughout the observational period (Fig. 6) and comparison with the median diel cycle shows a high bias in the model of a factor of ~ 2 . The observed hourly-averaged mean daily maximum is 91 pmol mol^{-1} , with a peak observed of $946 \text{ pmol mol}^{-1}$. The model

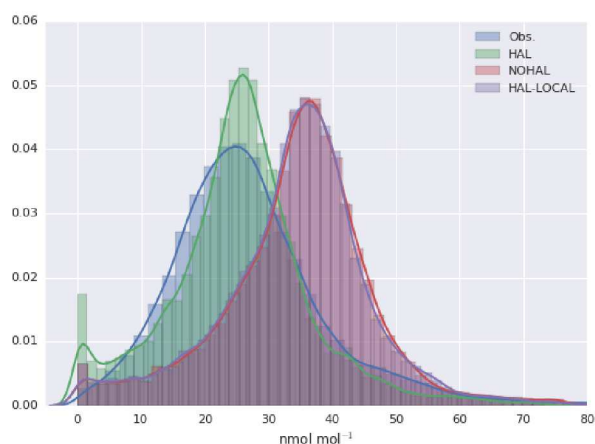


Fig. 4 Probability distribution function of observed and modelled O_3 mixing ratios at selected UK AURN background sites ($N=63$) for the observation period (29th June–1st August 2015). Modelled values are shown for the simulation with halogens (“HAL”), without halogens (“NOHAL”), and with halogens only with the European domain (“HAL-LOCAL”).

compares well in the mean maximum (95 pmol mol^{-1}). However modelled peak magnitude is around half the maximum observed value ($458 \text{ pmol mol}^{-1}$). The reactive uptake parameter used in the model for N_2O_5 on sea-salt aerosol is 0.005 for dry sea-salt (relative humidity less than 62 %) and 0.03 for wet sea-salt.⁸² However, if these values are reduced by half then we find a median peak mixing ratio of 37 pmol mol^{-1} , closer to the observations.

Molecular chlorine (Cl_2) was also measured at the site during the ICOZA campaign, but was found to be below the limit of detection ($8.5 \text{ pmol mol}^{-1}$). The model also does not predict mixing ratios above the limit of detection.

Observations of ClNO_2 have been made in London (51.5°N , -0.13°E)³³ and on a mountaintop near Frankfurt (50.22°N , 8.45°E)⁸³, with reported maximum nighttime values of 724 and $800 \text{ pmol mol}^{-1}$, respectively. The model calculates maximum nighttime mixing ratios of ~ 140 and $\sim 110 \text{ pmol mol}^{-1}$, for London and Frankfurt respectively and average nighttime maxima of ~ 40 and $\sim 30 \text{ pmol mol}^{-1}$. The model therefore has a significant negative bias to these inland ClNO_2 observations.

The published continental HCl observations show mixing ratios in the range of tens of pmol mol^{-1} to a few nmol mol^{-1} in Italy,⁸⁴ Netherlands,^{85,86} France,⁸⁷ Germany,⁸⁸ England,^{89–91} and Switzerland.⁹² The modelled mixing ratios peak at 12 pmol mol^{-1} . The model therefore significantly underestimates the HCl mixing ratios. Some of this bias is likely due to a lack of chlorine sources from anthropogenic activities both organic and inorganic and from aerosol processing of chloride. However, it may also reflect excessive loss processes for HCl.

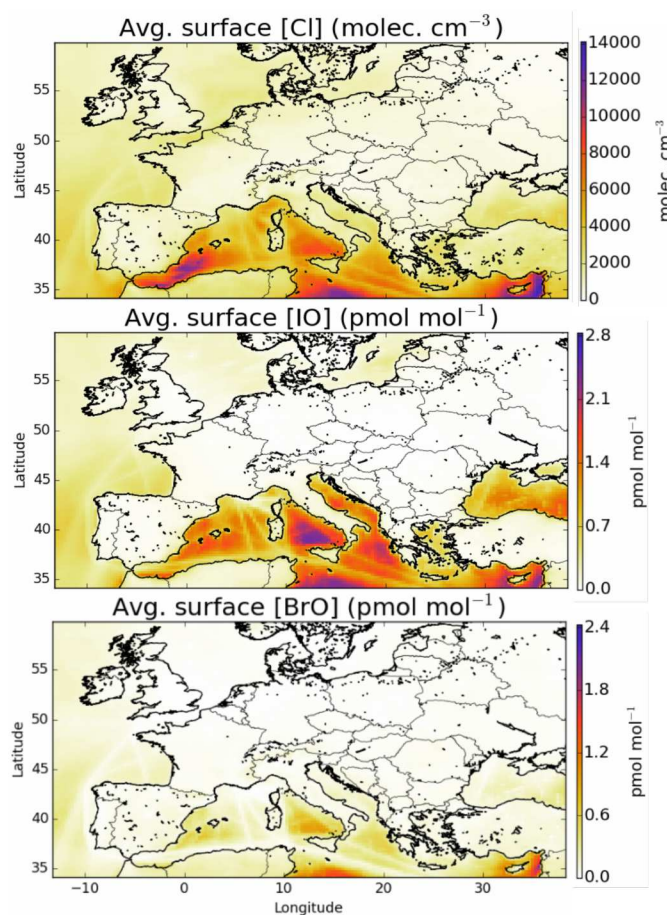


Fig. 5 Mean modelled surface mixing ratios of Cl, IO, and BrO during the observational period.

In summary the observational constraints on the modelled halogen concentrations are weak. Much of the observational activity has focussed on process level understanding of halogens at coastal hot spots. For these locations the model appears to systematically underestimate IO, OIO, I_2 and BrO mixing ratios. ClNO_2 mixing ratios inland appear to be underestimated. The model identifies the region with the most significant halogen chemistry as the Mediterranean, a region with a very low number of observations.

4 European ozone (O_3)

Figure 7 shows the difference in the mean surface O_3 mixing ratio between simulations with halogens (“HAL”) and without (“NOHAL”). O_3 reduces in all location and in some locations by a significant fraction (45 % or $28.9 \text{ nmol mol}^{-1}$). On average the surface O_3 within the domain drops by $13.5 \text{ nmol mol}^{-1}$ (25 %), consistent with previous studies.^{5,12,15,93}

To assess changes to O_3 within the domain’s boundary layer further, we consider the budget of the rapidly interchanging odd

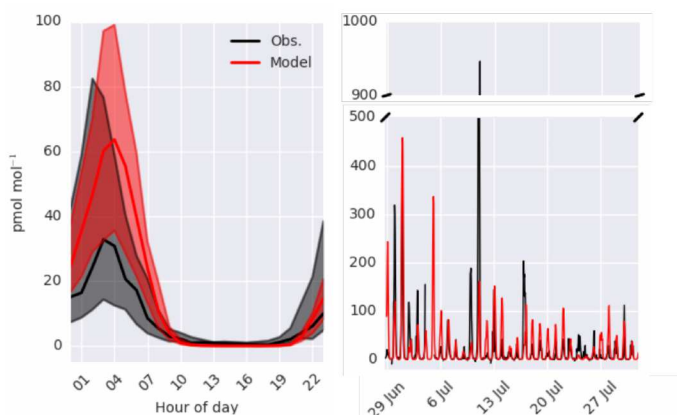


Fig. 6 Comparison of observed and modelled (“HAL”) CINO₂ as a median diel cycle (left) and timeseries (right) measured at Weybourne. Shaded region on diel plot give 25th and 75th percentiles.

oxygen species (O_x) (defined previously¹²). Table 2 gives an O_x budget for the boundary layer over Europe for the period of the observations (June 29th -August 1st 2015) for the simulations with (“HAL”) and without halogens (“NOHAL”). Inclusion of halogens leads to a slight decrease in the magnitude of the O_x sources of 4 %. This is predominantly due to a reduction in the mixing ratio of NO_x due to the hydrolysis of halogen nitrates ($\text{XNO}_3 \xrightarrow{\text{aq.}} \text{HOX} + \text{HNO}_3$, X=Cl, Br) as discussed on a global scale.^{11,12} The O_x sink term also decreases (7%) reflecting lower O₃ concentrations in the domain. The O_x chemical lifetime decreases from 8 days without halogens to 6.5 days with, a 20% reduction.

Table 2 Modelled odd oxygen (O_x¹²) budget within the European boundary layer (>900 hPa). Major losses and production routes are shown in units of Tg (O_x) per year scaled from the 34 days of simulation performed here. Values are rounded to one decimal place.

	“Cl+Br+I”	“NOHAL”
O ₃ burden (Tg)	0.9	1.2
NO + HO ₂	69.3	73.6
NO + RO ₂	40.8	41.3
Total chemical O _x sources	110.1	114.9
O ₃ + H ₂ O + hv	20.4	25.0
O ₃ + HO ₂	10.2	13.3
O ₃ + OH + O ₂	6.2	9.3
Bromine O _x sinks	1.1	0.0
Iodine O _x sinks	8.0	0.0
Chlorine O _x sinks	0.3	0.0
Total chemical O _x sinks	50.6	54.4
O ₃ Dry deposition	69	90

This reduction in the surface O₃ burden consists of two components: a reduction in the background O₃ entering the domain, predominantly from the West (the boundary conditions), and a change to the chemistry occurring within the domain.

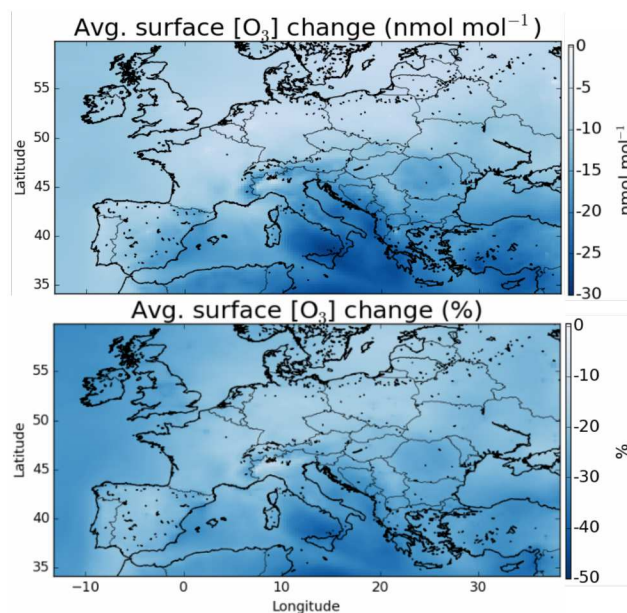


Fig. 7 Difference in surface mean O₃ mixing ratio between “HAL” and “NOHAL” in nmol mol⁻¹ (top) and percentage (bottom) terms over the simulation period.

By running a simulation with the boundary conditions from the global simulation without halogen chemistry, but with halogen chemistry occurring inside the domain (“HAL-LOCAL”) we can separate these two factors. Figure 8(top) shows the percentage decrease in the O₃ mixing ratio on inclusion of halogens (“HAL”-“NOHAL”)/“NOHAL”). The middle panel then shows the decrease which is attributable to the local chemistry (“HAL-LOCAL”-“NOHAL”)/“NOHAL”), with the bottom panel showing the difference between the two panels which we attribute to the global role of halogens in determining the boundary condition.

Over the northern and western part of the domain, the influence of halogens on the global mixing ratios (as manifested in the boundary conditions) dominates (Figure 8(bottom)). Mace Head (53.3°N, -9.9°E) on the west coast of Ireland is often used as the default background air quality site for North West Europe. O₃ at Mace Head drops by an average of 12 nmol mol⁻¹ (31 %) on the inclusion of halogen chemistry in both the boundary conditions and in the regional model (“HAL”) consistent with previous global studies.^{11,12,31} However, this reduction is only 0.51 nmol mol⁻¹ (1.3 %) in the simulation where the boundary condition doesn’t reflect global halogen chemistry (“HAL-LOCAL”). This influence of the reduced O₃ due to the a reduction in the global background, extends over the European Atlantic regions and into the North Sea. However, its magnitude decreases over continental regions especially in the south of the domain. This is due to the local production of O₃ in these regions and the shorter lifetime of O₃ in continental regions reducing the influence of boundary

conditions compared to marine regions.

Over the southern and eastern part of the domain the global background influence of halogens plays a less significant role and it is local halogen chemistry that dominates the reduction simulated in O_3 . For example over Sicily ($18.6^\circ N$, $14.2^\circ E$), O_3 mixing ratios are reduced $28.4 \text{ nmol mol}^{-1}$ (41 %) on the inclusion of halogen chemistry in both the boundary conditions and in the regional model (“HAL”) and by $24.3 \text{ nmol mol}^{-1}$ (35 %) in the simulation with only halogen chemistry occurring within the domain (“LOCAL”). Thus in this location the impact of halogens on the global background is much less important than the local halogen chemistry. Figure 5 shows much higher mixing ratios of halogens over the Mediterranean than any other region of the domain, however, there are no obvious observational constraints for halogen species here and so their regional influence is un-assessed.

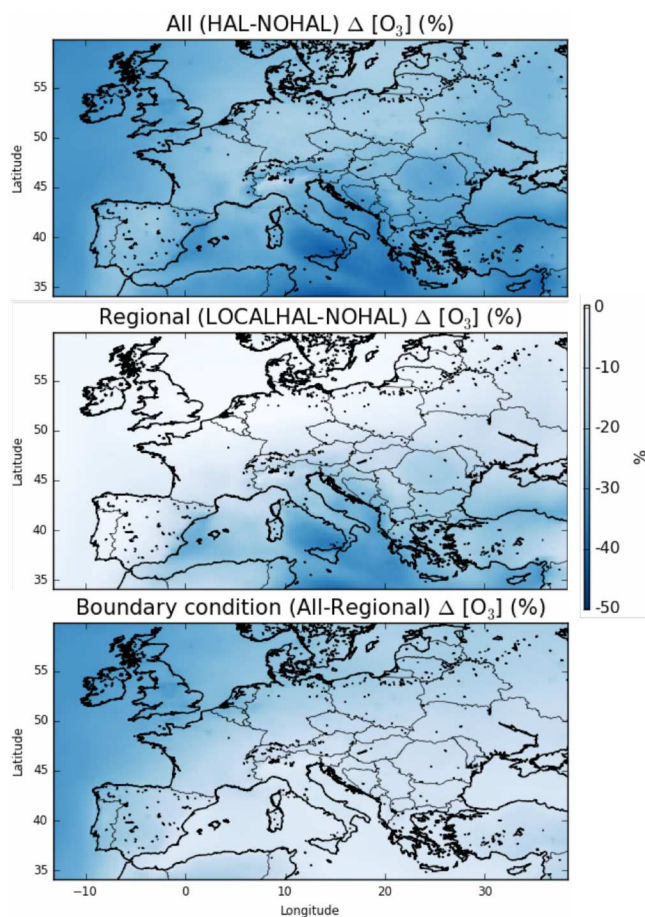


Fig. 8 Mean percentage difference in surface O_3 mixing ratio when halogens are included in all domains (“HAL” vs “NOHAL”, top), just within the European domain (“HAL-LOCAL” vs. “NOHAL”, middle), and the global contribution from the difference between these two (top-middle, at the bottom) plots.

The cumulative distribution functions of surface hourly O_3 mix-

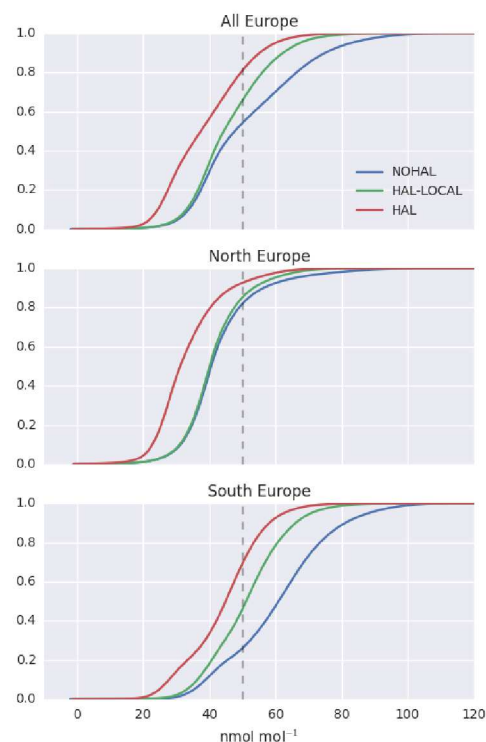


Fig. 9 Cumulative probability distribution plot of surface modelled O_3 for the observation period, for the entire domain (top), northern Europe ($>47^\circ N$, middle), and southern Europe ($<47^\circ N$, bottom). Modelled values are shown for the simulation with halogens (“HAL”), without halogens (“NOHAL”), and with halogens only with the European domain (“HAL-LOCAL”). Vertical dashed black line gives 50 nmol mol^{-1} . X axis is limited to $120 \text{ nmol mol}^{-1}$.

ing ratios over Europe for the differing simulations is shown in Figure 9. The inclusion of halogens reduces the probability of high O_3 occurring in the model but the difference between the north ($>47^\circ N$) and the south ($<47^\circ N$) of Europe is evident. For the north of Europe, only small changes are seen between simulations with only local halogens (“HAL-LOCAL”) compared to no halogens at all (“NOHAL”). The median O_3 mixing ratio in the north of Europe ($>47^\circ N$) are 31.1 , 40.0 , $40.5 \text{ nmol mol}^{-1}$ for the “HAL”, “HAL-LOCAL”, and “NOHAL” simulations respectively. Local chemistry thus plays little role in determining the median concentrations. However the role of local chemistry becomes more pronounced at the upper end of the O_3 distribution, with the 95^{th} percentile mixing ratios for these simulations being 54.0 , 59.4 , $65.6 \text{ nmol mol}^{-1}$.

For the south of Europe ($<47^\circ N$) a larger proportional of change between the simulation with halogens (“HAL”) and without (“NOHAL”), can be explained by local chemistry (“HAL-

LOCAL”) and this influence is felt throughout the O₃ distribution. Figure 9 shows a reduction in the median O₃ mixing ratio from “HAL” to “HAL-LOCAL” to “NOHAL” of 44.9, 51.1, 61.0 nmol mol⁻¹ respectively. Similar reductions can be seen in the 95th percentile mixing ratios with values of 62.4, 70.7, 88.1 nmol mol⁻¹.

The upper end of the O₃ distribution is most important from an air quality perspective. The model shows a decrease in average surface maximum mixing ratios of 19.9 nmol mol⁻¹ on inclusion of halogens. This is greater than the decrease seen in average surface mean mixing ratios (13.5 nmol mol⁻¹). For UK legislation, 50 nmol mol⁻¹ (100 μg m⁻³) is important for human health reasons as above this value exceedances are considered. 45.7 % of modelled surface O₃ values are above this value when halogens are not included (“NOHAL”), 34.12 % when halogens are just considered locally (“HAL-LOCAL”) and 18.9 % when halogens are considered in all domains (“HAL”). The O₃ mixing ratio of 40 nmol mol⁻¹ is considered important threshold for ecosystems⁹⁴. We see a decrease in the percent of hourly surface values above 40 nmol mol⁻¹ from 70.5 % in ‘NOHAL’, 65.9 % in “HAL-LOCAL”, to 43.3 % in “HAL”. Halogens reduce the percent of modelled values above 70 nmol mol⁻¹ too, with the values dropping from 15.1 % in “NOHAL” to 3.2 % in “HAL-LOCAL” and 0.9 % in “HAL”.

Within our model, with our current representation of halogen chemistry, and for the period we have investigated, halogens have a significant impact on the mixing ratio of modelled O₃. There are significant reductions in the mixing ratio of O₃ both in the north and south of Europe but for differing reasons (global background versus local chemistry) with influences both for the median and higher percentiles of the distribution. There is a need for significant and further evaluation of the model against an increased observation dataset to develop evidence to support these conclusions but this work suggest that halogens may play a significant role in determining the distribution of European surface O₃.

5 European oxidation

The oxidation of VOCs, CO, CH₄ in the presence of NO_x drives the chemistry of the troposphere. This oxidation is dominated by the OH radical. Within our domain we calculate average boundary layer OH concentrations of 3.53x10⁶, 3.08x10⁶, and 2.89x10⁶ molecules cm⁻³ for the simulations without halogens (“NOHAL”), with local halogens (“HAL-LOCAL”) and with global halogens (“HAL”) respectively.

The halogens tend to reduce OH mixing ratios (Figure 10) as they decrease O₃ and thus the production of OH via the primary sources (photolysis of ozone and the subsequent reactions of the photo products with water), and decrease the NO_x mixing ratio thus leading to smaller conversion of HO₂ to OH via this route (NO + HO₂). The conversion of HO₂ to OH via XO is not large

enough to compensate for this. This leads to an average reduction in surface OH mixing ratios of 16 %. The largest reductions are simulated where O₃ mixing ratios are reduced and where there is active halogen chemistry which leads to lower NO_x mixing ratios due to rapid hydrolysis of halogen nitrates on aerosol.

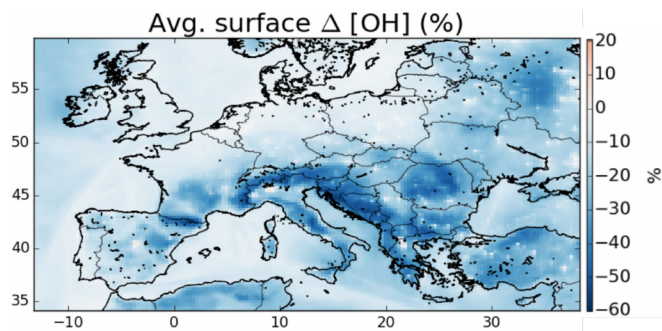


Fig. 10 Percentage difference in surface OH between simulation including halogens (“HAL”) and not (“NOHAL”).

The inclusion of halogen chemistry brings with it a new oxidant, atomic chlorine (Fig. 5). The average European boundary layer atomic chlorine mixing ratios is 2.1x10³ atoms cm⁻³. This compares with an annual averaged global tropospheric value of 1.3x10³ atoms cm⁻³ found by recent global modelling.⁷ Daytime modelled Cl mixing ratios at the surface range from 1.5x10² to 2.3x10⁴ atoms cm⁻³, with a maximum hourly value of 2.7x10⁵ atoms cm⁻³. Within the boundary layer atomic chlorine provides 12, 16 and 9.1 % of the sink for ethane, acetone and propane respectively. It contributes 1.7 % of the CH₄ loss. As discussed earlier a lack of observational constraint results in significant uncertainties in our simulation of Cl species but these simulations suggest that Cl may play a moderately important role in determining the oxidation of some VOCs within the European domain.

6 Chlorine versus bromine and iodine

Overall, we find that the combined impact of halogens (Cl, Br, I) leads to a reduction in O₃ mixing ratio over Europe. Previous studies investigating the impact of halogen species with comparable halogen schemes have come to similar conclusions.⁵ However, studies of chlorine, notably from ClNO₂, have found increases in O₃.²⁻⁴ In section 2.2 and 3.2 we show that the model likely provides a lower estimate for chlorine chemistry in the atmosphere, however it is instructive to examine the impact of ClNO₂ on the composition of the air over Europe.

The modelled mean-daily maximum mixing ratio of ClNO₂ is shown in Figure 11. Peak magnitudes are comparable to those reported in recent modelling work for Northern hemispheric summer of up to 400 pmol mol⁻¹,⁴ and annual values over Europe from global models of 100-140 pmol mol⁻¹.^{12,95} The highest regions for ClNO₂ mixing ratios are seen where shipping emissions

are greatest (Fig. 11). By running a simulation without ClNO_2 production ("NOCINO₂") the impact of ClNO_2 on O_3 can be assessed.

We find increases in O_3 surface mixing ratios on inclusion of ClNO_2 during summertime are modest as reported previously.^{2,4} The maximum increase seen in the average surface O_3 mixing ratio is up to 0.41 (1.2 %) nmol mol^{-1} , which is within the range of summer enhancement reported previously for the northern hemisphere (0.2-1.6 nmol mol^{-1}).⁴ Larger changes have been reported in winter time⁴ and would be expected if processes increasing chloride concentrations inland were included in the model.

In our model, the dominant source of reactive chlorine in the European boundary layer is the production of BrCl from heterogeneous routes,¹¹ rather than the production of ClNO_2 . This source is both more diffuse than the ClNO_2 source which requires high NO_x mixing ratios and does not decrease NO_x mixing ratios, in contrast to halogen nitrate hydrolysis. It seems likely therefore that when all chlorine sources are considered together they lead to a reduction in O_3 mixing ratios consistent with previous global studies.¹² Significant uncertainties remain in our fundamental understanding of this heterogeneous chlorine chemistry⁹⁶ and further laboratory and field studies are needed to clarify the mechanisms by which chlorine is released from sea-salt.

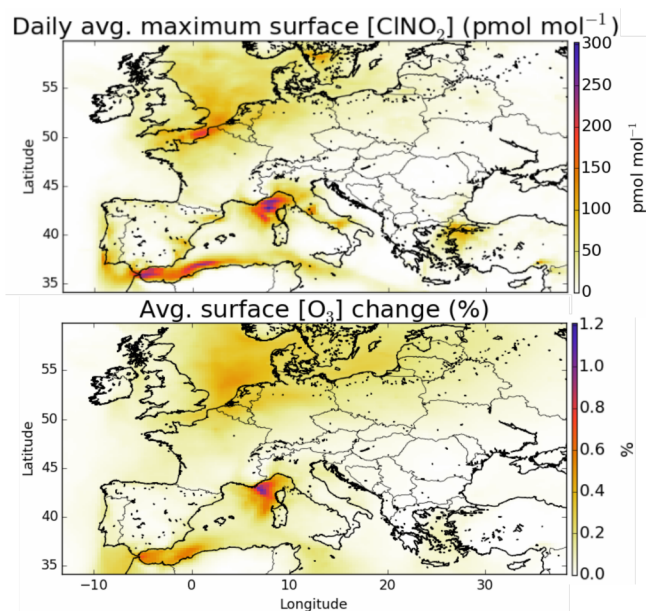


Fig. 11 Mean daily maximum surface ClNO_2 mixing ratios (top) and impact of ClNO_2 production on O_3 (bottom). Inclusion of ClNO_2 leads to small increases in the O_3 mixing ratio predominantly over coastal regions with heavy ship traffic.

7 Aerosols

Figure 12) shows the change in boundary layer fine particulate matter ($\text{PM}_{2.5}$), for all aerosol types and just for the sulfate (SO_4^{2-}), ammonia (NH_4^+), and nitrate (NO_3^-) system with and without halogens. The details of the calculation can be found in the supplementary information. These changes equate to a domain average decrease of 1.7 and 4.3 %, for $\text{PM}_{2.5}$ and $\text{SO}_4^{2-} + \text{NH}_4^+ + \text{NO}_3^-$ respectively. NO_3^- shows the largest changes in regions of higher altitude, highlighting the large decreases in NO_x seen at these altitudes on inclusion of halogens.^{11,12} Small changes are seen in the concentration of SO_4^{2-} reflecting the changes in the oxidants discussed in Section 5. However, halogens may be able to directly impact the production of SO_4^{2-} through the oxidation on aerosol of SO_2 by hypohalous acids (HOX) on aerosol has been discussed⁹⁷, which may lead to increased SO_4^{2-} production.

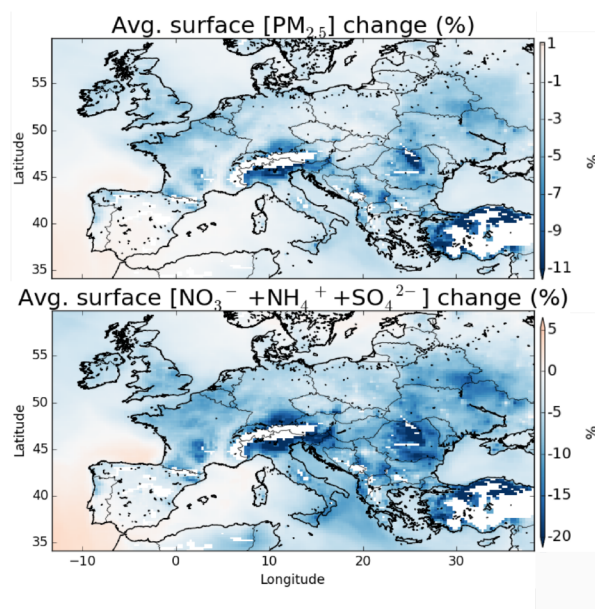


Fig. 12 Percentage difference in boundary layer surface (>900 hPa) total fine particulate matter (below 2.5 microns, $\text{PM}_{2.5}$), and the sulfate (SO_4^{2-}), ammonia (NH_4^+), and nitrate (NO_3^-) mode between the simulation with halogens ("HAL") and without ("NOHAL"). Maximum values on $\text{PM}_{2.5}$ and $\text{SO}_4^{2-} + \text{NH}_4^+ + \text{NO}_3^-$ plot are -21.1 and 34.9 %. Plotted regions are restricted to those with surface pressures greater than 900 hPa to remove larger influences at clean mountain top sites.

8 Conclusions and discussion

We have investigated the impact of Cl, Br and I chemistry on the mixing ratio of O_3 and other pollutants over Europe in the summer of 2015 using the GEOS-Chem model in its European configuration. An initial assessment of the model against observations made at the Weybourne Atmospheric Observatory and from

the UK air quality network shows some skill in capturing mean mixing ratios and diel cycle of O₃, NO₂, NO_y, and PM_{2.5} concentrations, however a more extensive assessment of the model in this configuration is needed. Comparisons between observations of ClNO₂ made at Weybourne, show a model over estimate on average. However, the model significantly underestimates ClNO₂ observations reported for more inland regions suggesting some missing processes. The mixing ratios of inorganic bromine and iodine species reported from European sites are significantly higher than those calculated. This likely reflects the the lack of realistic representation of coastal processes in the model.

Halogen chemistry has a significant impact on the O₃ mixing ratios calculated over Europe. The north of Europe is mainly sensitive to the reduction in the global O₃ background, whereas the south (notably the Mediterranean) is sensitive to the local halogen chemistry. Chlorine from ClNO₂ leads to a small regional increases in O₃ but this is overwhelmed by the decreases caused by the other halogens. We find that mean surface O₃ mixing ratios significantly reduced by an overage of 13.5 nmol mol⁻¹ (25 %), with the frequency of hourly mean surface O₃ mixing ratios above 50 nmol mol⁻¹ falling from 46 % to 18%. The frequency of occurrence of hourly mean surface ozone mixing ratios above 70 nmol mol⁻¹ falls from 15.1% to 0.9%. Halogen chemistry may therefore play an important role in determining the O₃ exposure over Europe. Oxidant mixing ratios are changed by halogens with OH at the surface dropping due to a reduction in primary production. Atomic Cl leads to some additional oxidation of VOCs notably for ethane, propane and acetone. Halogens appear to have little impact on aerosol mixing ratios.

Given these simulations it would appear that halogen chemistry may play a significant role in determining the O₃ mixing ratios found during summertime in Europe, and should be included in model analyses. Further studies are necessary to confirm these findings and to evaluate whether they have any specific relevance to European air quality policy. For example, do regions change from being NO_x or VOC limited on inclusion of the halogens? How does the model respond to future emissions scenarios? It would be surprising if Europe was alone in this sensitivity. Previous global model simulations¹² show other regions where halogens may play a role in determining the O₃ concentrations such as the west coast of the United States and Canada, western India, northern Japan, southern West Africa etc. Air quality simulations for these regions may similarly be sensitive to the inclusion and representation of halogen chemistry.

However, there is little observational constraint on these conclusions. The current set of observations of halogens in Europe are sparse and potentially biased by coastal specific processes. Future efforts to provide observations of atmospheric chlorine, bromine and iodine species in a range of environments, together with ocean iodide observations especially in the Mediterranean

would provide a useful constraint here. Continued development of the laboratory measurements especially of the heterogenous phase chemistry would also help to provide a better basis for these model simulations and our understanding of the role of halogen chemistry in determining air-quality.

9 Acknowledgements

We thank DEFRA for Weybourne and air-quality data from the Automatic Urban and Rural Network (AURN) and the National Centre for Atmospheric (NCAS) for access to observation made as part of their long-term measurement programme.

We thank the National Environment Research Council (NERC) for support through grants (NE/K004069/1, NE/K012398/1, NE/K012169/1) that supported the ICOZA and ClNO₂ project. LJC, MJE, and TMS also acknowledge support from NERC grants NE/N009983/1 and NE/L01291X/1.

We acknowledge the GEOS-Chem Support Team and the GEOS-Chem users community for their work developing and supporting the regional nested configurations of GEOS-Chem. In particular Junwei Xu for processing meteorological fields for the period of observations and Lee Murray for preparing lighting NO_x files for European grid.

References

- 1 W. R. Simpson, S. S. Brown, A. Saiz-Lopez, J. A. Thornton and R. von Glasow, *Chemical Reviews*, 2015, **115**, 4035–4062.
- 2 H. Simon, Y. Kimura, G. McGaughy, D. T. Allen, S. S. Brown, H. D. Osthoff, J. M. Roberts, D. Byun and D. Lee, *J Geophys. Res-Atmos.*, 2009, **114**, D00F03.
- 3 G. Sarwar, H. Simon, P. Bhave and G. Yarwood, *Atmos. Chem. Phys.*, 2012, **12**, 6455–6473.
- 4 G. Sarwar, H. Simon, J. Xing and R. Mathur, *Geophys. Res. Lett.*, 2014, **41**, 4050–4058.
- 5 G. Sarwar, B. Gantt, D. Schwede, K. Foley, R. Mathur and A. Saiz-Lopez, *Environ. Sci. Technol.*, 2015, **49**, 9203–11.
- 6 R. P. Fernandez, R. J. Salawitch, D. E. Kinnison, J.-F. Lamarque and A. Saiz-Lopez, *Atmos. Chem. Phys.*, 2014, **14**, 13391–13410.
- 7 R. Hossaini, M. P. Chipperfield, A. Saiz-Lopez, R. Fernandez, S. Monks, P. Brauer and R. von Glasow, *J Geophys. Res-Atmos.*, 2016.
- 8 J. P. Parrella, D. J. Jacob, Q. Liang, Y. Zhang, L. J. Mickley, B. Miller, M. J. Evans, X. Yang, J. A. Pyle, N. Theys and M. Van Roozendael, *Atmos. Chem. Phys.*, 2012, **12**, 6723–6740.
- 9 A. Saiz-Lopez, J. F. Lamarque, D. E. Kinnison, S. Tilmes, C. Ordóñez, J. J. Orlando, A. J. Conley, J. M. C. Plane, A. S. Mahajan, G. S. Santos, E. L. Atlas, D. R. Blake, S. P. Sander, S. Schauffler, A. M. Thompson and G. Brasseur, *Atmos. Chem. Phys.*, 2012, **12**, 3939–3949.
- 10 A. Saiz-Lopez, R. P. Fernandez, C. Ordóñez, D. E. Kinnison,

- J. C. Gómez Martín, J.-F. Lamarque and S. Tilmes, *Atmos. Chem. Phys.*, 2014, **14**, 19985–20044.
- 11 J. A. Schmidt, D. J. Jacob, H. M. Horowitz, L. Hu, T. Sherwen, M. J. Evans, Q. Liang, R. M. Suleiman, D. E. Oram, M. L. Breton, C. J. Percival, S. Wang, B. Dix and R. Volkamer, *J Geophys. Res-Atmos.*, 2016, 2169–8996.
- 12 T. Sherwen, J. A. Schmidt, M. J. Evans, L. J. Carpenter, K. Großmann, S. D. Eastham, D. J. Jacob, B. Dix, T. K. Koenig, R. Sinreich, I. Ortega, R. Volkamer, A. Saiz-Lopez, C. Prados-Roman, A. S. Mahajan and C. Ordóñez, *Atmos. Chem. Phys.*, 2016, **16**, 12239–12271.
- 13 T. Sherwen, M. J. Evans, L. J. Carpenter, J. A. Schmidt and L. J. Mickely, *Atmos. Chem. Phys. Discuss.*, 2016, 1–18.
- 14 T. E. Graedel and W. C. Keene, *Global Biogeochem. Cy.*, 1995, **9**, 47–77.
- 15 T. Sherwen, M. J. Evans, L. J. Carpenter, S. J. Andrews, R. T. Lidster, B. Dix, T. K. Koenig, R. Sinreich, I. Ortega, R. Volkamer, A. Saiz-Lopez, C. Prados-Roman, A. S. Mahajan and C. Ordóñez, *Atmos. Chem. Phys.*, 2016, **16**, 1161–1186.
- 16 J. Burkholder, J. P. D. Abbatt, R. E. Huie, M. J. Kurylo, D. M. Wilmouth, S. P. Sander, J. R. Barker, C. E. Kolb, V. L. Orkin and P. H. Wine, *Chemical Kinetics and Photochemical Data for Use in Atmospheric Studies - Evaluation Number 18*, Nasa panel for data evaluation technical report, 2015.
- 17 B. Alicke, K. Hebestreit, J. Stutz and U. Platt, *Nature*, 1999, **397**, 572–573.
- 18 C. Peters, S. Pechtl, J. Stutz, K. Hebestreit, G. Hönninger, K. G. Heumann, A. Schwarz, J. Winterlik and U. Platt, *Atmos. Chem. Phys.*, 2005, **5**, 3357–3375.
- 19 A. S. Mahajan, H. Oetjen, A. Saiz-Lopez, J. D. Lee, G. B. McFiggans and J. M. C. Plane, *Geophys. Res. Lett.*, 2009, **36**, L16803.
- 20 A. S. Mahajan, H. Oetjen, J. D. Lee, A. Saiz-Lopez, G. B. McFiggans and J. M. C. Plane, *Atmos. Environ.*, 2009, **43**, 3811–3818.
- 21 R. J. Leigh, S. M. Ball, J. Whitehead, C. Leblanc, A. J. L. Shillings, A. S. Mahajan, H. Oetjen, J. D. Lee, C. E. Jones, J. R. Dorsey, M. Gallagher, R. L. Jones, J. M. C. Plane, P. Potin and G. McFiggans, *Atmos. Chem. Phys.*, 2010, **10**, 11823–11838.
- 22 G. McFiggans, C. S. E. Bale, S. M. Ball, J. M. Beames, W. J. Bloss, L. J. Carpenter, J. Dorsey, R. Dunk, M. J. Flynn, K. L. Furneaux, M. W. Gallagher, D. E. Heard, A. M. Hollingsworth, K. Hornsby, T. Ingham, C. E. Jones, R. L. Jones, L. J. Kramer, J. M. Langridge, C. Leblanc, J.-P. LeCrane, J. D. Lee, R. J. Leigh, I. Longley, A. S. Mahajan, P. S. Monks, H. Oetjen, A. J. Orr-Ewing, J. M. C. Plane, P. Potin, A. J. L. Shillings, F. Thomas, R. von Glasow, R. Wada, L. K. Whalley and J. D. Whitehead, *Atmos. Chem. Phys.*, 2010, **10**, 2975–2999.
- 23 A. S. Mahajan, M. Sorribas, J. C. Gómez Martín, S. M. MacDonald, M. Gil, J. M. C. Plane and A. Saiz-Lopez, *Atmos. Chem. Phys.*, 2011, **11**, 2545–2555.
- 24 L. J. Carpenter, S. M. MacDonald, M. D. Shaw, R. Kumar, R. W. Saunders, R. Parthipan, J. Wilson and J. M. C. Plane, *Nature Geosci.*, 2013, **6**, 108–111.
- 25 S. M. MacDonald, J. C. Gómez Martín, R. Chance, S. Wariner, A. Saiz-Lopez, L. J. Carpenter and J. M. C. Plane, *Atmos. Chem. Phys.*, 2014, **14**, 5841–5852.
- 26 W. C. Keene, M. A. K. Khalil, D. J. Erickson, A. McCulloch, T. E. Graedel, J. M. Lobert, M. L. Aucott, S. L. Gong, D. B. Harper, G. Kleiman, P. Midgley, R. M. Moore, C. Seuzaret, W. T. Sturges, C. M. Benkovitz, V. Koropalov, L. A. Barrie and Y. F. Li, *J Geophys. Res-Atmos.*, 1999, **104**, 8429–8440.
- 27 A. McCulloch, M. L. Aucott, T. E. Graedel, G. Kleiman, P. M. Midgley and Y.-F. Li, *J Geophys. Res-Atmos.*, 1999, **104**, 8417–8427.
- 28 J. A. Thornton, J. P. Kercher, T. P. Riedel, N. L. Wagner, J. Cozic, J. S. Holloway, W. P. Dubé, G. M. Wolfe, P. K. Quinn, A. M. Middlebrook, B. Alexander and S. S. Brown, *Nature*, 2010, **464**, 271–274.
- 29 G. McFiggans, R. A. Cox, J. C. Mossinger, B. J. Allan and J. M. C. Plane, *J Geophys. Res-Atmos.*, 2002, **107**, ACH10–1–ACH10–10.
- 30 M. Ammann, R. A. Cox, J. N. Crowley, M. E. Jenkin, A. Mellouki, M. J. Rossi, J. Troe and T. J. Wallington, *Atmos. Chem. Phys.*, 2013, **13**, 8045–8228.
- 31 C. Prados-Roman, C. A. Cuevas, T. Hay, R. P. Fernandez, A. S. Mahajan, S.-J. Royer, M. Galí, R. Simó, J. Dachs, K. Großmann, D. E. Kinnison, J.-F. Lamarque and A. Saiz-Lopez, *Atmos. Chem. Phys.*, 2015, **15**, 583–593.
- 32 R. Volkamer, S. Baidar, T. Campos, S. Coburn, J. DiGangi, B. Dix, E. Eloranta, T. Koenig, B. Moley, I. Ortega, B. Pierce, M. Reeves, R. Sinreich, S.-Y. Wang, M. Zondlo and P. Romashkin, *Atmos. Meas. Tech.*, 2015, **8**, 623–687.
- 33 T. J. Bannan, A. M. Booth, A. Bacak, J. B. A. Muller, K. E. Leather, M. Le Breton, B. Jones, D. Young, H. Coe, J. Allan, S. Visser, J. G. Slowik, M. Furger, A. S. H. Prévôt, J. Lee, R. E. Dunmore, J. R. Hopkins, J. F. Hamilton, A. C. Lewis, L. K. Whalley, T. Sharp, D. Stone, D. E. Heard, Z. L. Fleming, R. Leigh, D. E. Shallcross and C. J. Percival, *J Geophys. Res-Atmos.*, 2015, **120**, 5638–5657.
- 34 C. B. Faxon, J. K. Bean and L. H. Ruiz, *Atmosphere*, 2015, **6**, 1487.
- 35 L. H. Mielke, A. Furgeson and H. D. Osthoff, *Environ. Sci. Technol.*, 2011, **45**, 8889–8896.
- 36 T. P. Riedel, N. L. Wagner, W. P. Dubé, A. M. Middlebrook, C. J. Young, F. Öztürk, R. Bahreini, T. C. VandenBoer, D. E. Wolfe, E. J. Williams, J. M. Roberts, S. S. Brown and J. A. Thornton, *J Geophys. Res-Atmos.*, 2013, **118**, 8702–8715.

- 37 T. P. Riedel, G. M. Wolfe, K. T. Danas, J. B. Gilman, W. C. Kuster, D. M. Bon, A. Vlasenko, S.-M. Li, E. J. Williams, B. M. Lerner, P. R. Veres, J. M. Roberts, J. S. Holloway, B. Lefer, S. S. Brown and J. A. Thornton, *Atmos. Chem. Phys.*, 2014, **14**, 3789–3800.
- 38 Y. J. Tham, C. Yan, L. Xue, Q. Zha, X. Wang and T. Wang, *Chin. Sci. Bull*, 2014, **59**, 356–359.
- 39 D. Chen, Y. Wang, M. B. McElroy, K. He, R. M. Yantosca and P. Le Sager, *Atmos. Chem. Phys.*, 2009, **9**, 3825–3839.
- 40 Y. X. Wang, M. B. McElroy, D. J. Jacob and R. M. Yantosca, *J Geophys. Res-Atmos.*, 2004, **109**, n/a–n/a.
- 41 L. Zhang, D. J. Jacob, N. V. Downey, D. A. Wood, D. Blewitt, C. C. Carouge, A. van Donkelaar, D. B. Jones, L. T. Murray and Y. Wang, *Atmospheric Environment*, 2011, **45**, 6769–6776.
- 42 L. Zhang, D. J. Jacob, E. M. Knipping, N. Kumar, J. W. Munger, C. C. Carouge, A. van Donkelaar, Y. X. Wang and D. Chen, *Atmos. Chem. Phys.*, 2012, **12**, 4539–4554.
- 43 G. C. M. Vinken, K. F. Boersma, D. J. Jacob and E. W. Meijer, *Atmospheric Chemistry and Physics*, 2011, **11**, 11707–11722.
- 44 C. Reed, C. A. Brumby, L. R. Crilley, L. J. Kramer, W. J. Bloss, P. W. Seakins, J. D. Lee and L. J. Carpenter, *Atmos. Meas. Tech.*, 2016, **9**, 2483–2495.
- 45 G. Forster, W. Sturges, Z. Fleming, B. Bandy and S. Emeis, *Tellus B*, 2012, **64**, 1–18.
- 46 C. Reed, M. J. Evans, P. Di Carlo, J. D. Lee and L. J. Carpenter, *Atmos. Chem. Phys.*, 2016, **16**, 4707–4724.
- 47 K. Clemmshaw, *Crit. Rev. Env. Sci Tec.*, 2004, **34**, 1–108.
- 48 F. C. Fehsenfeld, R. R. Dickerson, G. Hübler, W. T. Luke, L. J. Nunnermacker, E. J. Williams, J. M. Roberts, J. G. Calvert, C. M. Curran, A. C. Delany, C. S. Eubank, D. W. Fahey, A. Fried, B. W. Gandrud, A. O. Langford, P. C. Murphy, R. B. Norton, K. E. Pickering and B. A. Ridley, *J Geophys. Res-Atmos.*, 1987, **92**, 14710.
- 49 G. Villena, I. Bejan, R. Kurtenbach, P. Wiesen and J. Kleffmann, *Atmos. Meas. Tech.*, 2012, **5**, 149–159.
- 50 E. J. Williams, K. Baumann, J. M. Roberts, S. B. Bertman, R. B. Norton, F. C. Fehsenfeld, S. R. Springston, L. J. Nunnermacker, L. Newman, K. Olszyna, J. Meagher, B. Hartsell, E. Edgerton, J. R. Pearson and M. O. Rodgers, *J Geophys. Res-Atmos.*, 1998, **103**, 22261–22280.
- 51 D. L. Slusher, L. G. Huey, D. J. Tanner, F. M. Flocke and J. M. Roberts, *J. Geophys. Res.*, 2004, **109**, D19315.
- 52 J. Liao, H. Sihler, L. G. Huey, J. A. Neuman, D. J. Tanner, U. Friess, U. Platt, F. M. Flocke, J. J. Orlando, P. B. Shepson, H. J. Beine, A. J. Weinheimer, S. J. Sjostedt, J. B. Nowak, D. J. Knapp, R. M. Staebler, W. Zheng, R. Sander, S. R. Hall and K. Ullmann, *J. Geophys. Res.*, 2011, **116**, D00R02.
- 53 R. D. Thaler, L. H. Mielke and H. D. Osthoff, *Anal Chem*, 2011, **83**, 2761–2766.
- 54 DEFRA, *Department for Environment Food & Rural Affairs - Automatic Urban and Rural Network Data* - downloaded via *OpenAir*.
- 55 D. C. Carslaw and K. Ropkins, *Environ. Modell. Softw.*, 2012, **27–28**, 52–61.
- 56 J. Mao, F. Paulot, D. J. Jacob, R. C. Cohen, J. D. Crouse, P. O. Wennberg, C. A. Keller, R. C. Hudman, M. P. Barkley and L. W. Horowitz, *J Geophys. Res-Atmos.*, 2013, **118**, 11,256–11,268.
- 57 T. D. Fairlie, D. J. Jacob, J. E. Dibb, B. Alexander, M. A. Avery, A. van Donkelaar and L. Zhang, *Atmospheric Chemistry and Physics*, 2010, **10**, 3999–4012.
- 58 L. Jaeglé, P. K. Quinn, T. S. Bates, B. Alexander and J. T. Lin, *Atmos. Chem. Phys.*, 2011, **11**, 3137–3157.
- 59 S. D. Eastham, D. K. Weisenstein and S. R. H. Barrett, *Atmos. Environ.*, 2014, **89**, 52–63.
- 60 J. M. Roberts, H. D. Osthoff, S. S. Brown, A. R. Ravishankara, D. Coffman, P. Quinn and T. Bates, *Geophys. Res. Lett.*, 2009, **36**, L20808.
- 61 A. B. Guenther, X. Jiang, C. L. Heald, T. Sakulyanontvittaya, T. Duhl, L. K. Emmons and X. Wang, *Geoscientific Model Development*, 2012, **5**, 1471–1492.
- 62 G. R. van der Werf, J. T. Randerson, L. Giglio, G. J. Collatz, M. Mu, P. S. Kasibhatla, D. C. Morton, R. S. DeFries, Y. Jin and T. T. van Leeuwen, *Atmospheric Chemistry and Physics*, 2010, **10**, 11707–11735.
- 63 R. Yevich and J. A. Logan, *Global Biogeochemical Cycles*, 2003, **17**, n/a–n/a.
- 64 T. C. Bond, E. Bhardwaj, R. Dong, R. Jogani, S. Jung, C. Roden, D. G. Streets and N. M. Trautmann, *Global Biogeochemical Cycles*, 2007, **21**, n/a–n/a.
- 65 L. T. Murray, D. J. Jacob, J. A. Logan, R. C. Hudman and W. J. Koshak, *J Geophys. Res-Atmos.*, 2012, **117**, D20307.
- 66 R. C. Hudman, N. E. Moore, A. K. Mebust, R. V. Martin, A. R. Russell, L. C. Valin and R. C. Cohen, *Atmospheric Chemistry and Physics*, 2012, **12**, 7779–7795.
- 67 M. Stettler, S. Eastham and S. Barrett, *Atmospheric Environment*, 2011, **45**, 5415–5424.
- 68 V. Vestreng, L. Ntziachristos, A. Semb, S. Reis, I. S. A. Isaksen and L. Tarrasón, *Atmos. Chem. Phys.*, 2009, **9**, 1503–1520.
- 69 V. Vestreng, G. Myhre, H. Fagerli, S. Reis and L. Tarrasón, *Atmos. Chem. Phys.*, 2007, **7**, 3663–3681.
- 70 R. E. Dunmore, L. K. Whalley, T. Sherwen, M. J. Evans, D. E. Heard, J. R. Hopkins, J. D. Lee, A. C. Lewis, R. T. Lidster, A. R. Rickard and J. F. Hamilton, *Faraday Discuss.*, 2016, **189**, 105–120.
- 71 C. Ordóñez, J. F. Lamarque, S. Tilmes, D. E. Kinnison, E. L. Atlas, D. R. Blake, G. S. Santos, G. Brasseur and A. Saiz-Lopez, *Atmos. Chem. Phys.*, 2012, **12**, 1423–1447.
- 72 E. E. Agency.

- 73 K. L. Furneaux, L. K. Whalley, D. E. Heard, H. M. Atkinson, W. J. Bloss, M. J. Flynn, M. W. Gallagher, T. Ingham, L. Kramer, J. D. Lee, R. Leigh, G. B. McFiggans, A. S. Mahajan, P. S. Monks, H. Oetjen, J. M. C. Plane and J. D. Whitehead, *Atmos. Chem. Phys.*, 2010, **10**, 3645–3663.
- 74 B. J. Allan, G. McFiggans, J. M. C. Plane and H. Coe, *Journal of Geophysical Research: Atmospheres*, 2000, **105**, 14363–14369.
- 75 R. Commane, K. Seitz, C. S. E. Bale, W. J. Bloss, J. Buxmann, T. Ingham, U. Platt, D. Pöhler and D. E. Heard, *Atmospheric Chemistry and Physics*, 2011, **11**, 6721–6733.
- 76 M. Bitter, S. M. Ball, I. M. Povey and R. L. Jones, *Atmos. Chem. Phys.*, 2005, **5**, 2547–2560.
- 77 H. Oetjen, *PhD thesis*, University of Bremen, Germany, 2009.
- 78 A. Saiz-Lopez and J. M. C. Plane, *Geophys. Res. Lett.*, 2004, **31**, L04112.
- 79 R. J. Huang, K. Seitz, J. Buxmann, D. Pöhler, K. E. Hornsby, L. J. Carpenter, U. Platt and T. Hoffmann, *Atmos. Chem. Phys.*, 2010, **10**, 4823–4833.
- 80 A. Saiz-Lopez, J. M. C. Plane and J. A. Shillito, *Geophys. Res. Lett.*, 2004, **31**, L03111.
- 81 H. Leser, G. Hönninger and U. Platt, *Geophys. Res. Lett.*, 2003, **30**, 1537.
- 82 M. J. Evans and D. J. Jacob, *Geophys. Res. Lett.*, 2005, **32**, L09813.
- 83 G. J. Phillips, M. J. Tang, J. Thieser, B. Brickwedde, G. Schuster, B. Bohn, J. Lelieveld and J. N. Crowley, *Geophys. Res. Lett.*, 2012, **39**, L10811.
- 84 I. Allegrini, F. Santis, A. Febo, A. Liberti and M. Posanzini, *Physico-Chemical Behaviour of Atmospheric Pollutants*, Springer Netherlands, 1984, pp. 12–19.
- 85 J.-W. Erisman, A. W. Vermetten, W. A. Asman, A. Waijers-Ijpelaan and J. Slanina, *Atmos. Environ.*, 1988, **22**, 1153–1160.
- 86 M. P. Keuken, R. P. Otjes and J. Slanina, in *Simultaneously Sampling of NH₃, HNO₃, HNO₂, HCl, SO₂ And H₂O₂ in Ambient Air by A Wet Annular Denuder System*, ed. G. Restelli and G. Angeletti, Springer Netherlands, Dordrecht, 1990, pp. 92–97.
- 87 P. Marché, A. Barbe, C. Secroun, J. Corr and P. Jouve, *Geophys. Res. Lett.*, 1980, **7**, 869–872.
- 88 P. Matusca, B. Schwarz and K. Bächmann, *Atmos. Environ.*, 1984, **18**, 1667–1675.
- 89 N. Dimmock and G. Marshall, *Anal. Chim. Acta*, 1987, **202**, 49–59.
- 90 W. T. Sturges and R. M. Harrison, *Atmos. Environ.*, 1989, **23**, 1987–1996.
- 91 R. M. Harrison and A. Allen, *Atmos. Environ. Part A. General Topics*, 1990, **24**, 369–376.
- 92 C. Johnson, L. Sigg and J. Zobrist, *Atmos. Environ.*, 1987, **21**, 2365–2374.
- 93 G. Sarwar, D. Kang, K. Foley, D. Schwede, B. Gantt and R. Mathur, 2016, DOI: 10.1016/j.atmosenv.2016.06.072.
- 94 J.-P. Tuovinen, *Environmental Pollution*, 2000, **109**, 361–372.
- 95 M. S. Long, W. C. Keene, R. C. Easter, R. Sander, X. Liu, A. Kerkweg and D. Erickson, *Atmos. Chem. Phys.*, 2014, **14**, 3397–3425.
- 96 R. Sommariva and R. von Glasow, *Environ. Sci. Technol.*, 2012, **46**, 10429–10437.
- 97 Q. Chen, L. Geng, J. A. Schmidt, Z. Xie, H. Kang, J. Dachs, J. Cole-Dai, A. J. Schauer, M. G. Camp and B. Alexander, *Atmos. Chem. Phys.*, 2016, **16**, 11433–11450.